Lasing properties of InP/$(Ga_{0.51}In_{0.49})$P quantum dots in microdisk cavities

M. Witzany, R. Roßbach, W.-M. Schulz, M. Jetter, and P. Michler
Institut für Halbleiteroptik und Funktionelle Grenzflächen, Universität Stuttgart, D-70569 Stuttgart, Germany

T.-L. Liu and E. Hu
School of Engineering and Applied Sciences, Harvard University, Cambridge, Massachusetts 02138, USA

J. Wiersig
Institut für Theoretische Physik, Otto-von-Guericke-Universität Magdeburg, Postfach 4120, D-39016 Magdeburg, Germany

F. Jahnke
Institut für Theoretische Physik, Universität Bremen, Postfach 330 440, D-28334 Bremen, Germany
(Received 11 August 2010; revised manuscript received 25 January 2011; published 10 May 2011)

We investigated the photoluminescence from InP quantum dots incorporated in $(Ga_{0.51}In_{0.49})$P microdisk structures. With increasing pump power we observe a transition to stimulated emission indicated by the S shape of the input-output curve. This transition is accompanied with a concentration of the emission to one or a few modes exhibiting quality factors on the order of 10^4 at transparency. Time-resolved measurements show that at the same time the photoluminescence decay time considerably decreases. Furthermore, in the transition regime the linewidth of the lasing mode is reduced and the second-order photon correlation function exhibits a reduction of fluctuations as previously reported for lasers with InAs quantum dots in photonic crystal, microdisk and micropillar cavities as the gain medium. The experimental findings are compared with the predictions of a microscopic theory.

DOI: 10.1103/PhysRevB.83.205305 PACS number(s): 78.67.Hc, 42.55.Sa, 42.50.Ar, 78.55.Cr

I. INTRODUCTION

Whispering-gallery modes (WGMs) have been introduced by Lord Rayleigh already in 1910 to describe the propagation of sound waves.[1] On a length scale orders of magnitude smaller, WGMs have been used in 1961 to explain the propagation of maser emission in spherical samples of Samarium doped CaF_2 (Ref. 2). Another 31 years later, semiconductor-based whispering-gallery mode microdisk lasers using InGaAs quantum wells as the active medium have been introduced.[3] Since then the comparatively easy processing and the high quality factors (Q) over broad spectral widths have largely promoted the examination of microdisks (MD) in the perspective of miniaturized low-threshold semiconductor lasing devices. The application of an inhomogeneously broadened quantum dot (QD) ensemble as the gain medium in microdisk structures[4,5] allows for lasing on distinct modes spread over a wide spectral range. Until today, quantum dot lasing from microdisk structures has been reported for various material systems. So far, the lower and upper bounds of the wavelength range for microdisk QD lasing are given by (In_xGa_{1-x})As QDs in (Al_xGa_{1-x})As microdisks (∼1300 nm) and CdSe QDs in ZnSe microdisks (∼520 nm), respectively.[6,7] Most thoroughly investigated is the material system with (In_xGa_{1-x})As QDs incorporated in GaAs or (Al_xGa_{1-x})As microdisks. In these structures lasing has been achieved through modes from 900 to 1300 nm exhibiting Q factors in excess of 3×10^5, see Ref. 6. Recently, laser emission in the visible red (∼750 nm) was reported for InP QDs in GaInP waveguide microdisks ($Q \sim 2-5 \times 10^3$), see Ref. 8.

In this paper, we present results for the laser emission from InP QDs embedded in wet-etched free standing $(Ga_{0.51}In_{0.49})$P microdisks with Q factors of up to 1.6×10^4 under pulsed optical excitation. The QDs in our sample emit in the spectral range of 660–675 nm where fast Si avalanche photo diodes show the highest sensitivity. We could perform time-correlated photon counting (TCPC) measurements on disks with diameters of 4 and 9 μm. With this we trace the behavior of the QD photoluminescence (PL) decay dynamics with increasing pump power to values well above the transition into stimulated emission. Moreover, an in-depth investigation of the regime of the onset of stimulated emission reveals both a distinct decrease of the lasing mode linewidth and a gradual transition of the second-order correlation value at zero delay from photon-bunching toward the characteristic Poissonian statistics of laser emission. These investigations are in good agreement with the theoretical predictions and complement recent measurements performed on lasers consisting of InAs QDs in photonic crystal,[9] microdisk,[10] and micropillar cavities.[11]

II. SAMPLE AND EXPERIMENT

The sample was grown on a (100) silicon-doped GaAs substrate tilted toward the [111]A direction by 6°. Using metal-organic vapor-phase epitaxy (MOVPE), initially, a 100-nm buffer GaAs layer was deposited followed by a short period superlattice consisting of 30.5 pairs of 7 nm GaAs:Si and 7 nm $(Al_{0.5}Ga_{0.5})$As:Si finally topped by 200 nm GaAs. The superlattice shall provide a smoothened surface for the following layers. As a sacrificial layer for the aluminum selective wet-etching process 1 μm of $(Al_{0.5}Ga_{0.5})$As was grown. For the QDs serving as the active layer 2.1 monolayers (ML) of InP were deposited at a growth rate of 1.05 ML/s and a reactor temperature of 710°C. These growth conditions

lead to a monomodal narrow height distribution of the QDs with a maximum at 5.5 nm. The spectral distribution of the PL has a maximum at about 1.85 eV. The structural density is approximately 1.5×10^{10} cm^{-2}. The QDs are embedded in a separate-confinement heterostructure (SCH) consisting of a symmetric arrangement of a 10 nm $(Ga_{0.51}In_{0.49})P$ layer, a 20 nm $(Al_{0.5}Ga_{0.5})InP$ and a 67 nm layer of $(Ga_{0.51}In_{0.49})P$, all lattice matched to GaAs, to ensure both electronic and optical confinement. The active layer together with the SCH constitutes the actual microdisk after the etching process. Further information on the growth procedure of the QDs can be obtained from Ref. 12.

The microdisk structuring process started with the formation of disk patterns with diameters of 5 and 10 μm by optical lithography using an i-line stepper. A resist reflow process at 160°C was then applied for 90 s to smooth the pattern edges. The initial patterns were etched through the post material by a wet chemical etch comprising $HBr/H_2O/K_2Cr_2O_7$. This wet etch is crystallographically isotropic and therefore the disk diameter is reduced by approximately 1 μm resulting in structural diameters of 4 and 9 μm. The resist was then removed and the $Al_{0.5}Ga_{0.5}As$ sacrificial layer was selectively etched in 80° AZ300T resist stripper. This wet chemical process provides a crystallographic etch of the arsenide-based post material with no measurable thinning of the phosphidic disk layer. Compared with the widely used hydrofluoric acid (HF) the AZ300T resist stripper does not attack the $(Al_{0.5}Ga_{0.5})InP$ layers and provides a more precisely controlled etching (∼600 nm per 30 min). The etching process resulted in high quality structures, examples of which are shown in Fig. 1.

For optical investigations, the samples were mounted in a low-temperature (5 K) confocal microphotoluminescence (μPL) setup. A piezoelectrically adjustable microscope with a 50 times objective was used to both focus the incident laser beam to a spot diameter of approximately 1.5 μm and collect the emerging μPL from the top of the MD. The cryostat is mounted on a xy-stepper providing spatial lateral scanning capability with a resolution of 50 nm each. We excited the sample using a fiber laser generating a supercontinuum from 470 to 1800 nm. From the supercontinuum 2-nm wide pulses at 600-nm (∼2.1 eV) pulses with a temporal full width at half maximum (FWHM) of 4 ps and a repetition rate of 50 MHz were selected using an acoustooptic tunable filter. The collected PL was then dispersed via a 500-mm monochromator with a 1200 or a 1800 l/mm grating. To spectrally investigate the signal a thermoelectrically cooled(−70°) charge-coupled device (CCD) camera was used. The overall spectral resolution

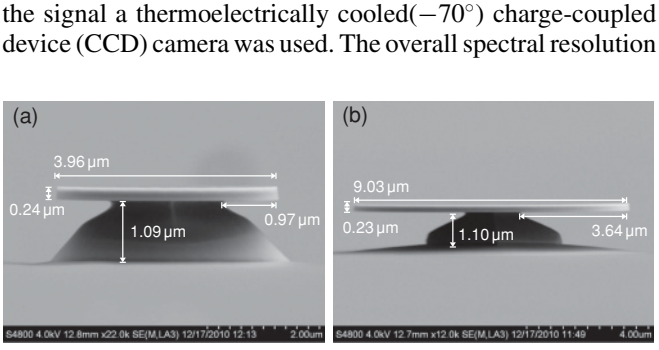

FIG. 1. Scanning electron microscopy picture of (a) a 4-μm diameter MD and (b) a 9-μm diameter MD.

was ∼200 μeV with the 1200 l/mm grating and ∼110 μeV with the 1800 l/mm grating, respectively. Photon statistics measurements in terms of the autocorrelation function

$$g^{(2)}(\tau = 0) = \frac{\langle b^\dagger b^\dagger b b \rangle}{\langle b^\dagger b \rangle^2}, \quad (1)$$

with the photon creation and annihilation operators $b^\dagger$, b of the laser mode were performed with a Hanbury-Brown and Twiss (HBT) setup[13] consisting of a 50/50 beam splitter and two high quantum efficiency avalanche photo diodes (APDs) within two orthogonal detection paths. Each APD provides a timing resolution of 600 ps. To perform time-correlated photon counting (TCPC) measurements, we used a high-speed APD with a typical timing resolution of 40 ps. Both photon-statistics measurements are based on analog time-to-amplitude (TAC) conversion and subsequent digital-to-analogue (D/A) conversion via a 4096 multichannel analyzer (MCA).

To acquire polarization resolved data the sample was mounted in a different setup under a tilt angle of 10° with respect to the vertical direction. This enabled us to pump the MDs from the top while collecting the PL from the side of the disk under an angle of 10°. We analyzed the linear polarization of the PL via its projection onto an orthogonal linear polarization basis using a rotatable half-wave plate mounted in front of a polarizing beam splitter.

III. EXPERIMENTAL RESULTS

To analyze both the mode structure and the quality factor of the microdisk structures with different diameters in detail, μPL spectra were taken at various excitation powers. Figure 2 illustrates spectra of a 4-μm and a 9-μm diameter microdisk at excitation powers well below and above the lasing thresholds. The displayed optical modes are computed by solving Maxwell's equations in the frequency domain in terms of Bessel/Hankel functions in the radial direction and trigonometric/exponential functions in the azimuthal and the vertical direction. The factorization of the vertical and the in-plane contributions is assumed within the effective index approach.[14] In our calculations we take into account the considerable dispersion of $(Ga_{0.51}In_{0.49})P$ and $(Al_{0.5}Ga_{0.5})InP$ in the spectral region of interest. The modes are labeled TE/TM(x,y) where TE/TM indicates whether the electric or the magnetic field component is parallel to the disk plane and x and y are the azimuthal and the radial mode number, respectively.

For low excitation powers, in the case of the 4-μm diameter microdisk [Fig. 2(a)], we observe one dominant line at ∼680.3 nm which we assign to the transverse electric WGM TE(52,1). Furthermore, we see several peaks assigned to WGMs of higher radial order surrounded by a spectrally broad contribution from QD ensemble PL. At an excitation power well above the laser threshold shown in the lower part of Fig. 2(a) we observe emission mainly through a mode at 671.7 nm that could be identified as TE(53,1) and only a very small contribution from the mode dominating at the low excitation power. In Fig. 2(b) we compare these results with the characteristic emission of a 9-μm diameter microdisk. For low excitation powers we do not observe any dominant mode emission but the spectrally broadened signal of the

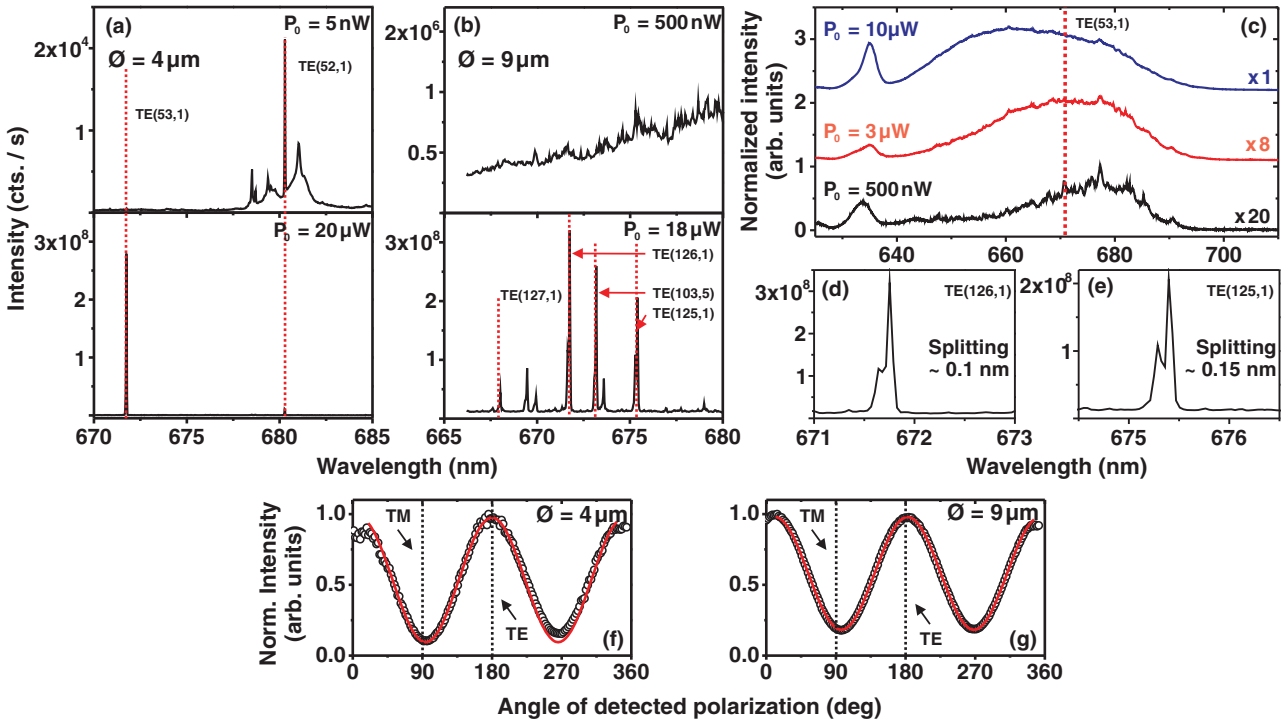

FIG. 2. (Color online) μPL spectra of (a) a 4-μm diameter and (b) a 9-μm diameter microdisk. The upper graphs display the situation for an excitation power (P_0) below the lasing threshold, the lower graphs show emission spectra above the laser threshold. The red-dashed lines mark the spectral position of calculated WGMs. Subfigure (c) shows PL spectra recorded from an unprocessed region of the sample for three different excitation powers. Subfigures (d) and (e) contain closeups of the modes TE(126,1) and TE(125,1) from the lower part of (b). (f) and (g) show polarization-resolved data for the mode TE(53,1) from the 4 μm and the mode TE(125,1) from the 9-μm diameter MD. The black dotted lines indicate the expected direction of polarization for TE- and TM-polarized modes, respectively. The red solid curves shall serve as guides to the eye.

QD ensemble. At high excitation powers we obtain emission through various narrow modes. As illustrated in Figs. 2(d) and 2(e), the lines identified as TE(126,1) and TE(125,1) exhibit a doublet structure with a splitting of about 0.1 nm (~300 μeV) and 0.15 nm (~400 μeV), respectively. We interpret this splitting to be due to a coupling between ideally degenerate counterpropagating WGMs that occurs because of backscattering on microscopic cavity defects.[15,16] For both the 4-μm and the 9-μm diameter structures, modes on the high energy side of the QD ensemble are favored. This can be accounted to a state filling with increasing excitation power which is a well known effect in InP QDs.[17] To support this assumption we recorded a series of three PL spectra taken from an unprocessed region of the sample for three different excitation powers as displayed in Fig. 2(c). The center of the PL emission is found to shift toward shorter wavelengths with increasing excitation power. In QD ensembles this is a clear indication for state filling. The same blue shift of the laser emission with respect to the peak of the ensemble luminescence at low excitation powers has also been observed in other QD lasing devices of different material systems.[18,19] A power-dependent TCPC measurement series taken from the same unprocessed region of the sample, however, does not show the typical decrease in PL lifetime expected from predominant excited state recombination in InP QDs.[17] Hence, we attribute the prevailing part of the lasing gain to s-shell recombination with some contribution from excited state recombination of unknown quantity. The peak at 635 nm corresponds to the ($Ga_{0.51}In_{0.49}$)P barrier emission.

To support our mode assignment we did a polarization analysis of the identified modes. In Figs. 2(f) and (g) the modes TE(53,1) and TE(125,1) serve as an example for the results we obtained for the identified modes from 4-μm and a 9-μm diameter disks, respectively. Both modes exhibit a strong TE polarization of $(82 \pm 2)\%$ and $(71 \pm 2)\%$. The degree of polarization was calculated using

$$P = \frac{I_{\max} - I_{\min}}{I_{\max} + I_{\min}} = \frac{I_{\mathrm{TE}} - I_{\mathrm{TM}}}{I_{\mathrm{TE}} + I_{\mathrm{TM}}}, \qquad (2)$$

where $I_{\max} = I_{\mathrm{TE}}$ and $I_{\min} = I_{\mathrm{TM}}$ denote the intensities for TE- and TM-polarized emission. This result is in good agreement with both our mode calculations and the previously reported strong TE polarization of InP QD containing laser devices.[20] Taking into account the spectral density of the QDs in the active region and the size of the microdisks, we estimate the number of QDs contributing to the spectra to be ~40 for the 4-μm and ~200 for the 9-μm diameter disks. In practice, probably more QDs contribute to the emission spectra due to nonresonant dot cavity coupling.[21,22] Both the number of contributing QDs and the spectral spacing of microdisk modes, which is considerably smaller for the 9-μm diameter microdisks, account for the difference in the high power excitation spectra.

To estimate the cavity quality factors of the investigated modes we tracked the power dependence of the emission

linewidth. In general, the quality factor Q_{tot} can be written as

$$Q_{\text{tot}}^{-1} = Q_{\text{mode}}^{-1} + Q_{\text{abs}}^{-1} + Q_{\text{loss}}^{-1}, \tag{3}$$

with Q_{mode}^{-1} determined by the intrinsic radiative loss of a mode in a perfect cavity, Q_{abs}^{-1} as the loss rate due to reabsorption by the active medium, and Q_{loss}^{-1} caused by cavity imperfections such as surface roughness (see, e.g., Ref. 23). In the low excitation power regime, bleaching of the absorption of the active medium with increasing excitation power leads to a decreasing linewidth. Approaching transparency absorption losses become negligible. Our model calculations predict transparency to occur at approximately 1.6 μW of pump power [data point marked with a red ellipse in Fig. 4(c)]. At this point, the observed linewidth allows a good estimation of $Q_{\text{mode}}^{-1} + Q_{\text{loss}}^{-1}$, that is, the quality factor of the mode in the nonperfect, realistic cavity. Using the relation $Q \sim E/\Delta E$, where E denotes the absolute mode energy and ΔE the spectral linewidth of the mode, the quality factor for the mode TE(53,1) in Fig. 2(a) is $16\,300 \pm 700$. For two of the three dominantly lasing modes in lower Fig. 2(b) we find $Q_{\text{TE}(126,1)} = (15\,000 \pm 500)$ and $Q_{\text{TM}(125,1)} = (13\,400 \pm 600)$. The Q factor of the mode TE(103,5) could not be determined because the mode was overlaid by the ensemble PL at transparency. We would like to note that the measured linewidths are on the order of the resolution limit of our setup. Therefore, the stated Q factors are to be interpreted as lower bounds.

In Fig. 3 the above-discussed spectrally resolved data are complemented by two power-dependent TCPC series to examine the time dependence of the mode emission. The measurements were performed on two modes of a 4-μm (a) and a 9-μm microdisk mode (b), respectively. In either case, the μPL was spectrally prefiltered to the mode bandwidth, and the excitation power was varied over approximately three orders of magnitude. For low excitation powers both the 4-μm and the 9-μm diameter microdisk modes exhibit a mainly monoexponential decay behavior revealing lifetimes of (450 ± 20) ps and (420 ± 20) ps, respectively.

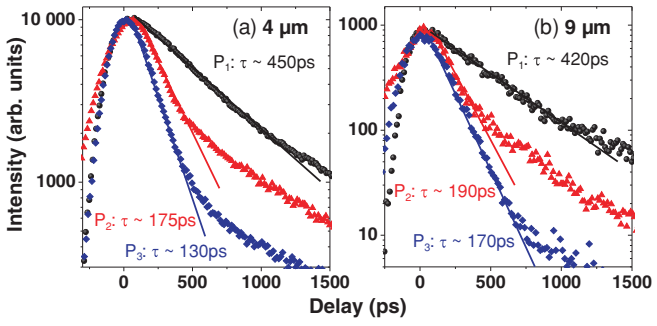

FIG. 3. (Color online) Time evolution of the μPL intensity for three different excitation powers of a mode from a microdisk with (a) 4-μm diameter [TE(53,1)] and (b) 9-μm diameter [TE(103,5)]. The black circles represent the time trace for below threshold excitation [$P_1 = 0.4\mu\text{W}/1\mu\text{W}$ for (a) / (b)], the red triangles for a excitation power close to the onset of lasing ($P_2 = 4\ \mu\text{W}/12\ \mu\text{W}$), the blue diamonds for an excitation power well above the lasing threshold ($P_3 = 8\,\mu\text{W}/50\,\mu\text{W}$). The τ values correspond to an exponential fit (indicated by the solid lines) to the data.

Increasing the excitation power to intermediate values, both the 4-μm and the 9-μm microdisk mode significantly change their time traces. The decay of about the first order of magnitude of the PL is found to be strongly accelerated resulting in lifetimes of (175 ± 20) ps for the 4-μm and (190 ± 20) ps for the 9-μm diameter structure. The decay traces also exhibit a slower decay component with rates that resemble those of the low power excitation case. For high excitation powers the fast decay contribution is further accelerated to (130 ± 20) ps and (170 ± 20) ps, respectively. The slowly decaying contribution now accounts for a fraction of less than 0.05 of the total PL. The lifetimes for the case of low excitation powers are consistent with those of time-resolved measurements on bare InP QDs without a cavity and corresponds well with the average lifetime of neutral excitonic recombination in these types of QDs.[17] In this low power regime, we hence mainly observe spontaneous emission. We do not observe any Purcell effect as the lifetime of the PL from the 4-μm diameter microdisk mode conforms to the PL lifetime of the mode originating from the 9-μm diameter microdisk within the accuracy of the experiment. We interpret the significant decrease of lifetime for intermediate and high excitation powers for the dominant fraction of the PL as a consequence of the transition from spontaneous to stimulated emission.

In the following we present details of the emission characteristics of single microdisk modes with special attention to the transition regime between dominant spontaneous and dominant stimulated emission. Representative data from a 4-μm diameter microdisk is depicted in Fig. 4 where the transition regime is highlighted by the blue shaded area. The measurements and analysis include μPL power series, a power-dependent series of HBT autocorrelations and mode linewidths as well as TCPC measurements of the μPL lifetime. In Fig. 4(a) the input-output characteristics of the lasing mode TE(53,1) is plotted. In a double logarithmic representation of the integrated mode intensity versus the pump power one can perceive an s-shaped smooth intensity transition for intermediate values of the excitation power. Such an input-output graph progression is characteristic for small mode volume semiconductor microcavity lasers.[8,11,24,25] The very small offset between the nonlasing and the lasing regime slopes of less than one order of magnitude also suggests a β value (i.e., a high spontaneous emission coupling ratio[26]) well above conventional lasers with 10^{-5} typically.

Figure 4(b) depicts the Poisson-normalized values $g^{(2)}(\tau = 0)$ versus the pump power. These values were extracted from a power-dependent series of pulsed HBT autocorrelation measurements by integrating the zero delay peak and comparing to the expectation value of a Poissonian light source of the same strength. In the inset in Fig. 4(b) side peaks displaced by $\tau = n \cdot \Delta t_{\text{exc}}$ represent correlation events between photons from consecutive excitation cycles. For a laser pulse repetition rate of 50 MHz we get $t_{\text{exc}} = 20$ ns which is far above the intrinsic lifetime of InP QD excitons. We can therefore assume that all peaks apart from $\tau = 0$ denote only uncorrelated events which obey Poissonian statistics. To only record the photon statistics of the lasing mode the μPL was spectrally prefiltered to a bandwidth of approximately 0.6 nm (1.6 meV) including the complete mode μPL. At about 2 μW pump power (i.e.,

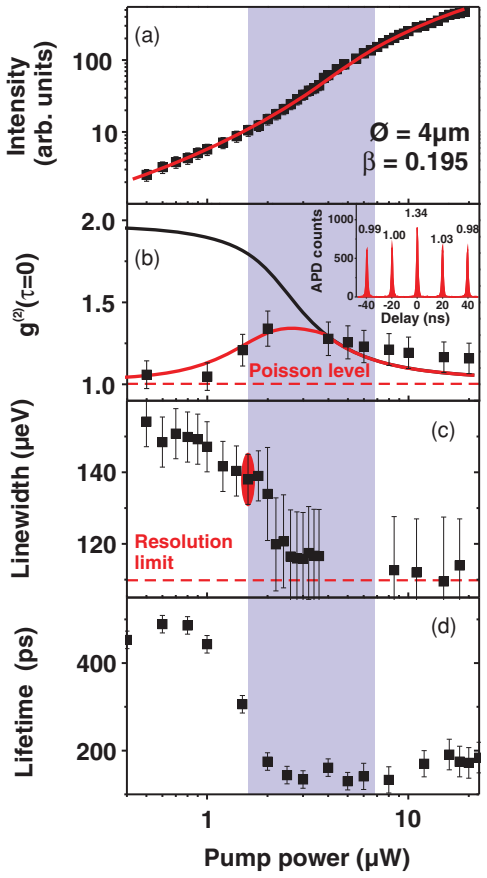

FIG. 4. (Color online) Lasing properties of a 4-μm diameter microdisk. (a) The output intensity plotted double logarithmically. The red line represents simulation data. (b) The progression of $g^{(2)}(0)$. The black line represents simulation data for a HBT setup with an infinite temporal resolution. The red line represents simulation data under consideration of the finite temporal resolution of the experiment setup. The inset shows a histogram containing the raw data from a correlation measurement at an excitation power of 2 μW. (c) The linewidth obtained from a Gaussian fit to the recorded μPL data. The red dashed line symbolizes the resolution limit. We applied greater error bars when the fitted values approach the resolution limit of the μPL detection setup. The red solid ellipse marks the data point which was used for the Q-factor estimation. (d) The lifetime of the main decay component of the μPL. The blue area highlights the region were lasing sets in.

within the pump power regime which can be identified as the onset of lasing due to the characteristic superlinear increase in the I/O curve) we observe a strong signature of photon bunching. This is manifested by a value of $g^{(2)}(\tau = 0) > 1$ in contrast to the correlation peaks at long delays. For increasing pump power this value of $g^{(2)}(\tau = 0)$ is found to decrease and approach unity as expected for the Poissonian photon statistics of stabilized laser emission. This behavior of $g^{(2)}(\tau = 0)$ at the lasing transition has previously been reported for photonic crystal,[9] microdisk,[10] and micropillar[11] lasers. Below the threshold though $g^{(2)}(\tau = 0)$ remains close to unity despite the expected thermal behavior of a mode fed through spontaneously emitting QDs.[27] In accordance with Ref. 11 we account this observation as a consequence of the limited temporal resolution of our HBT setup. This basic limit for photon statistics measurements set by the timing accuracy of APDs has recently been overcome by using a specially adapted streak camera as the detector.[25] As illustrated in Fig. 4(c) also the mode emission linewidth is subject to a substantial decrease in parallel with the onset of stimulated emission. This linewidth narrowing is explainable in terms of the Schawlow-Townes[28] model that predicts a reciprocal proportionality $\Delta E \sim 1/P_0$ to the optical power output of the lasing mode. Since a strong increase in the emitted optical power occurs around the lasing threshold, the observed decrease of the lasing mode's linewidth is expected. We like to note that the linewidth narrowing could only be traced over a limited range of excitation powers until ΔE drops below the resolution limit of our setup.

Figure 4(d) displays values of the lifetime of the dominant decay component of the 4-μm diameter microdisk mode extracted from a power-dependent TCPC series. In this disk the decrease of the decay time runs ahead of the other indications for the inset of stimulated emission.

IV. THEORY

The I/O curves and the second-order autocorrelation function (1) are calculated by using a recently developed semiconductor theory.[29] From the microscopic Hamiltonian for the interacting carrier-photon system the time evolution of the carrier population and the photon number using Heisenberg's equations of motion is determined. The arising hierarchy of equations is truncated by means of the cluster expansion scheme.[30] The autocorrelation function (1) can be written in terms of the correlation function

$$\delta\langle b^\dagger b^\dagger bb\rangle = \langle b^\dagger b^\dagger bb\rangle - 2\langle b^\dagger b\rangle^2 , \tag{4}$$

which is fourth order in the cluster expansion

$$g^{(2)}(0) = 2 + \delta\langle b^\dagger b^\dagger bb\rangle/\langle b^\dagger b\rangle^2 . \tag{5}$$

For a self-consistent theory on this level, we start with equations of motion for the photon number $\langle b^\dagger b\rangle$ and the electron and hole populations, $f_\nu^e = \langle c_\nu^\dagger c_\nu\rangle$ and $f_\nu^h = 1 - \langle v_\nu^\dagger v_\nu\rangle$, respectively, where ν is the electronic state index of second-quantization carrier operators. The source term of these equations contains the photon-assisted polarization $\langle b^\dagger v_\nu^\dagger c_\nu\rangle$, which introduces the additional carrier-photon correlations $\delta\langle b^\dagger b c_\nu^\dagger c_\nu\rangle$ and $\delta\langle b^\dagger b v_\nu^\dagger v_\nu\rangle$. Their dynamics, as well as the equation of motion for $\delta\langle b^\dagger b^\dagger bb\rangle$, are coupled to $\delta\langle b^\dagger b^\dagger b v_\nu^\dagger c_\nu\rangle$, for which another dynamical equation is solved. Coulomb effects are restricted to renormalized interband couplings, effective transition energies and scattering rates to explain the basic features of the presented experimental results.

For the calculations, we distinguish between the laser mode and nonlasing modes. The equation of motion for the photon-assisted polarization of the nonlasing modes is eliminated adiabatically to introduce the β factor. We consider QDs with two confined shells. The laser transition is the s-shell recombination. As the excitation condition we assume carrier injection into the barrier or wetting layer states with rapid carrier capture into the QDs. In such an incoherent excitation regime the pump process can be modeled with a constant carrier generation rate P in the p shell, incorporating saturation effects due to Pauli blocking. We consider fast carrier scattering from the p to the s shell in relaxation

time approximation.[31] Furthermore, rates for cavity losses and damping of polarization-like correlations are introduced.

Figure 4(a) provides a comparison of the numerical and experimental results for the I/O curve of the MD with a diameter of 4 μm. We considered 140 resonant QDs with damping $\gamma = 0.58$ meV, and a spontaneous emission time of 300 ps. The β and quality factors are set to be $\beta = 0.195$ and $Q = 35\,800$. With these parameter values we find a very good agreement of theoretical and experimental data. Note that such large values of the β factor have been also observed in other quantum dot microdisk lasers.[32–34] Microdisk lasers with quantum wells as active medium have usually lower β factors (see e.g., Ref. 35) as they couple more efficiently to leaky modes localized near the center region of the disk.

Figure 4(b) shows the corresponding autocorrelation function $g^{(2)}(0)$ as function of pump power computed for the same parameter set. It exhibits a smooth transition from a value of about 2 indicating thermal light emission below the laser threshold to a value of about 1 corresponding to coherent light well above threshold. To correctly describe the experimental correlation traces $\tilde{g}^{(2)}(\tau)$ under consideration of the HBT setup temporal resolution $\Delta t_{IRF} \approx 600$ ps we compute a convolution of $g^{(2)}(\tau)$ with a Gaussian function of width $2\sigma = \Delta t_{IRF}$ as

$$\tilde{g}^{(2)}(\tau) = 1/\sqrt{2\pi\sigma^2} \int_{-\infty}^{\infty} d\tau' g^{(2)}(\tau - \tau') \exp(-\tau'^2/2\sigma^2). \tag{6}$$

For the autocorrelation function we assume a time dependence as for thermal light

$$g^{(2)}(\tau) = 1 + [g^{(2)}(0) - 1] \exp(-2|\tau|/\tau_c). \tag{7}$$

We require, moreover, that τ_c can be approximated by the first-order coherence time which we compute as in Ref. 36. The convoluted $\tilde{g}^{(2)}(\tau = 0)$ is shown as red line in Fig. 4(b). It agrees well with the experimental data, including the correlation "peak" near threshold.

V. SUMMARY

In summary, we performed spectrally and temporally resolved PL measurements on InP QDs embedded in free standing wet-etched $(Ga_{0.51}In_{0.49})P$ microdisks at different excitation powers. By solving the Maxwell equations in the frequency domain for the microdisk resonators and comparing the obtained spectra with the experimental data various WGM modes could be identified. The modes exhibit Q factors of up to 1.6×10^4. With increasing excitation powers we observed a transition into stimulated emission for both a 4-μm and a 9-μm microdisk. Using the example of the 4-μm microdisk we performed an in-depth analysis of the lasing transition in terms of the optical output, the autocorrelation function $g^{(2)}(\tau)$, the lasing mode's linewidth, and the PL decay time. All investigated parameters show a typical behavior in the transition region and are in good accordance with previously published investigations of QD-based microcavity lasing devices. In a comparison of the predictions of a microscopic semiconductor theory with the experimental data we found a high consistency and determined the β factor of the microcavity laser to be as high as 0.195.

ACKNOWLEDGMENTS

The authors gratefully acknowledge funding by the DFG via the Forschergruppe 730.

[1] Lord Rayleigh, Philos. Mag. **20**, 1001 (1910).
[2] C. Garrett, W. Kaiser, and W. Bond, Phys. Rev. **124**, 1807 (1961).
[3] S. L. McCall, A. F. J. Levi, R. E. Slusher, S. J. Pearton, and R. A. Logan, Appl. Phys. Lett. **60**, 289 (1992).
[4] H. Cao, J. Y. Xu, W. H. Xiang, Y. Ma, S.-H. Chang, S. T. Ho, and G. S. Solomon, Appl. Phys. Lett. **76**, 3519 (2000).
[5] P. Michler, A. Kiraz, L. Zhang, C. Becher, E. Hu, and A. Imamoglu, Appl. Phys. Lett. **77**, 184 (2000).
[6] K. Srinivasan, M. Borselli, T. J. Johnson, P. E. Barclay, O. Painter, A. Stintz, and S. Krishna, Appl. Phys. Lett. **86**, 151106 (2005).
[7] J. Renner, L. Worschech, A. Forchel, S. Mahapatra, and K. Brunner, Appl. Phys. Lett. **89**, 231104 (2006).
[8] Y. Chu, A. Mintairov, Y. He, J. Merz, N. Kalyuzhnyy, V. Lantratov, and S. Mintairov, Phys. Lett. A **373**, 1185 (2009).
[9] S. Strauf, K. Hennessy, M. T. Rakher, Y.-S. Choi, A. Badolato, L. C. Andreani, E. L. Hu, P. M. Petroff, and D. Bouwmeester, Phys. Rev. Lett. **96**, 127404 (2006).
[10] Z. G. Xie, S. Götzinger, W. Fang, H. Cao, and G. S. Solomon, Phys. Rev. Lett. **98**, 117401 (2007).
[11] S. M. Ulrich, C. Gies, S. Ates, J. Wiersig, S. Reitzenstein, C. Hofmann, A. Löffler, A. Forchel, F. Jahnke, and P. Michler, Phys. Rev. Lett. **98**, 043906 (2007).
[12] W.-M. Schulz, R. Roßbach, M. Reischle, G. J. Beirne, M. Bommer, M. Jetter, and P. Michler, Phys. Rev. B **79**, 035329 (2009).
[13] R. Hanbury-Brown and R. Q. Twiss, Nature (London) **177**, 27 (1956).
[14] M. Borselli, T. Johnson, and O. Painter, Opt. Express **13**, 1515 (2005).
[15] D. S. Weiss, V. Sandoghdar, J. Hare, V. Lefèvre-Seguin, J.-M. Raimond, and S. Haroche, Opt. Lett. **20**, 1835 (1995).
[16] K. Srinivasan and O. Painter, Phys. Rev. A **75**, 023814 (2007).
[17] G. J. Beirne, M. Reischle, R. Roßbach, W.-M. Schulz, M. Jetter, J. Seebeck, P. Gartner, C. Gies, F. Jahnke, and P. Michler, Phys. Rev. B **75**, 195302 (2007).
[18] S. Fafard, K. Hinzer, S. Raymond, M. Dion, J. McCaffrey, Y. Feng, and S. Charbonneau, Science **274**, 1350 (1996).
[19] W.-M. Schulz, M. Eichfelder, R. Roßbach, M. Jetter, and P. Michler, Appl. Phys. Express **2**, 112501 (2009).
[20] T. Riedl, E. Fehrenbacher, M. K. Zundel, K. Eberl, and A. Hangleiter, Jpn. J. Appl. Phys. **38**, 597 (1999).
[21] K. Hennessy, A. Badolato, M. Winger, D. Gerace, M. Atatüre, S. Gulde, S. Fält, E. L. Hu, and A. Imamoglu, Nature (London) **445**, 896 (2007).

[22]S. Ates, S. M. Ulrich, A. Ulhaq, S. Reitzenstein, A. Löffler, S. Höfling, A. Forchel, and P. Michler, Nature Photon. **3**, 724 (2009).
[23]R. E. Slusher, A. F. J. Levi, U. Mohideen, S. L. McCall, S. J. Pearton, and R. A. Logan, Appl. Phys. Lett. **63**, 1310 (1993).
[24]S. Reitzenstein, A. Bazhenov, A. Gorbunov, C. Hofmann, S. Münch, A. Löffler, M. Kamp, J. P. Reithmaier, V. D. Kulakovskii, and A. Forchel, Appl. Phys. Lett. **89**, 051107 (2006).
[25]J. Wiersig, C. Gies, F. Jahnke, M. Aßmann, T. Berstermann, M. Bayer, C. Kistner, S. Reitzenstein, C. Schneider, S. Höfling *et al.*, Nature (London) **460**, 245 (2009).
[26]G. Björk and Y. Yamamoto, IEEE J. Quantum Electron. **27**, 2386 (1991).
[27]P. R. Rice and H. J. Carmichael, Phys. Rev. A **50**, 4318 (1994).
[28]A. Schawlow and C. Townes, Phys. Rev. **112**, 1940 (1958).
[29]C. Gies, J. Wiersig, M. Lorke, and F. Jahnke, Phys. Rev. A **75**, 013803 (2007).
[30]J. Fricke, Ann. Phys. (NY) **252**, 479 (1996).
[31]T. R. Nielsen, P. Gartner, and F. Jahnke, Phys. Rev. B **69**, 235314 (2004).
[32]K. Srinivasan, M. Borselli, O. Painter, A. Stintz, and S. Krishna, Opt. Express **14**, 1094 (2006).
[33]J. Renner, L. Worschech, A. Forchel, S. Mahapatra, and K. Brunner, Appl. Phys. Lett. **89**, 231104 (2006).
[34]W. H. Wang, S. Ghosh, F. M. Mendoza, X. Li, D. D. Awschalom, and N. Samarth, Phys. Rev. B **71**, 155306 (2005).
[35]J. Vucković, O. Painter, Y. Xu, A. Yariv, and A. Scherer, IEEE J. Quantum Electron. **35**, 1168 (1999).
[36]S. Ates, C. Gies, S. M. Ulrich, J. Wiersig, S. Reitzenstein, A. Löffler, A. Forchel, F. Jahnke, and P. Michler, Phys. Rev. B **78**, 155319 (2008).